JMEPEG (2011) 20:1620–1630
DOI: 10.1007/s11665-010-9822-y

1059-9495/$19.00

Fatigue Performance of Gas Tungsten Arc, Electron Beam, and Laser Beam Welded Ti-6Al-4V Alloy Joints

T.S. Balasubramanian, V. Balasubramanian, and M.A. Muthumanikkam

(Submitted June 26, 2010; in revised form August 23, 2010)

Titanium alloys have been successfully applied for aerospace, ship, and chemical industries because they possess many good characteristics such as high strength to weight ratio, superior corrosion resistance, and excellent high temperature resistance. Though these alloys show reasonable weldability characteristics, the joint properties are greatly influenced by the welding processes. The evaluation and prediction of fatigue life are very important for the welded joints to avoid catastrophic failure particularly in titanium alloys. This article compares the fatigue performance of Ti-6Al-4V alloy fabricated by gas tungsten arc welding, laser beam welding, and electron beam welding processes. The resultant fatigue properties of the welded joints are correlated with the tensile properties and microstructural characteristics. Of the three processes considered the joint welded by laser beam welding exhibits higher fatigue limit when compared with the other two processes due to the presence of fine lamellar microstructure in the weld metal region.

Keywords electron beam welding, fatigue, gas tungsten arc welding, laser beam welding, microstructure, titanium alloy

1. Introduction

In current industrial practice, welds and welded joints are an integral part of many complex load-carrying structures. Unfortunately, welds are often the weakest portions of these structures and their quality directly affects the integrity of the structure (Ref 1). Failure analysis of the weldments has indicated that fatigue alone accounts for most of the disruptive failures. Thus, welding is a major factor in the fatigue lifetime reduction of components. As fatigue failure is one of the prime concerns in structural design and the butt weld is a part of many structures, its evaluation and prediction of fatigue life is very important to avoid catastrophic failure particularly in titanium alloys. Titanium alloys have been successfully applied for aerospace, ship, desalination of sea water, and chemical industries because they possess many good characteristics such as high strength to weight ratio, corrosion resistance, toughness, low thermal expansion rate, high temperature creep resistance, and good formability (Ref 2-4).

Presently, Ti-6Al-4V is one of the most widely used titanium alloys, accounting for more than half of all titanium tonnage in the world, and no other titanium alloys threaten its dominant position (Ref 5, 6). Ti-6Al-4V alloy is commonly used in nuclear engineering, civil industries and medically implanted materials, transportable bridge girders, military vehicles, road tankers, and space vehicles, for its above-said significant properties (Ref 7, 8). The welding technology of titanium is complicated due to the fact that at temperatures above 550 °C, and particularly in the molten stage, it is known to be very reactive with atmospheric gases such as oxygen, nitrogen, carbon, or hydrogen causing severe embrittlement (Ref 9). Gas tungsten arc welding (GTAW) is a preferred welding method for reactive materials like titanium alloy due to its comparatively easier applicability and better economy (Ref 7). Laser beam welding (LBW) has been used for welding of titanium alloys due to its advantages such as precision and noncontact processing, with a small HAZ, consistent and reliable joints, etc. (Ref 10). Electron beam welding (EBW) is highly suited for joining titanium, as the high vacuum inside the chamber where the process is carried out, shields hot metal from contamination (Ref 11). The other advantages of the EBW process are deeper and narrower welds, low heat input (narrow heat-affected zone), high depth to width ratio (eliminates multi pass welds), higher welding speeds (reduces time to finish the joining process), increases productivity and higher energy efficiency (Ref 12).

Fatigue crack growth behavior in a welded $\alpha + \beta$ Ti-Al-Mn alloy in relation to the microstructural features was investigated by Keshava Murthy et al. (Ref 13). It was reported that, a significant increase in fatigue crack growth resistance due to the presence of tensile residual stress normal to the fatigue load in addition with lamellar microstructure. Saxena et al. (Ref 14) studied the effect of phase morphology on fatigue crack growth behavior of $\alpha + \beta$ titanium alloy and reported that the fatigue crack growth is strongly influenced by the phase morphology. The effect of notch size in high cycle fatigue behavior of Ti-6Al-4V alloy was studied by Haritos et al. (Ref 15) on bars and plates. Results indicate that while there is a definite notch size effect in the Ti-6Al-4V bar within the range of notch sizes tested, little or no such effect exists in the plate. The reasons were discussed as the state of stress at the root of notch in cylindrical specimen was biaxial whereas in plate, a reduced

T.S. Balasubramanian and **M.A. Muthumanikkam**, Combat Vehicle Research and Development Establishment (CVRDE), Avadi, Chennai 600 054, India; and **V. Balasubramanian**, Department of Manufacturing Engineering, Center for Materials Joining Research (CEMAJOR), Annamalai University, Annamalainagar 608 002, Tamil Nadu, India. Contact e-mails: tsbraja@yahoo.com, visvabalu@yahoo.com, and mamuthumanickam@yahoo.com.

state of plane strain at the notch root will be contrasted with the cylindrical specimen. No single parameter is adequate for characterizing the notch effect, other parameters shall be considered are material condition, notch root radius, local stress field, and notch root plasticity. The role of residual stresses in the high cycle fatigue (HCF) strength of Ti-6Al-4V subjected to foreign object damage (FOD) was evaluated by Thompson et al. (Ref 16), and reported that generally, stress relief improves the fatigue limit stress. Stress relief removes the tensile residual stress, since tensile residual stresses led to degradation of the fatigue behavior. Boyce.et al. (Ref 17) investigated that the influence of load ratio and maximum stress intensity and found that crack growth and threshold are independent of loading frequency up to 50-1000 Hz. The fatigue thresholds were found to vary significantly with positive load ratio ($R = 0.1 - 0.95$). At load ratios larger than R_c, i.e., $R \sim 0.5$-0.95, where (global) crack closure could no longer be detected, a different dependence of the ΔK_{th} threshold on load ratio was seen, with $\Delta K_{th} \rightarrow 0$ as $R \rightarrow 1$.

Tsay et al. (Ref 18) explored the influence of porosity on the fatigue crack growth behavior of Ti-6Al-4V alloy laser welds and concluded that at a lower stress ratio, the effect of porosity against fatigue crack growth resistance is less when compared to a higher stress ratio. Zuo et al. (Ref 19) reported that the *S-N* curves of Ti-6Al-4V with the bimodal and basket weave microstructures continuously decrease with increasing the number of cycles to failure and have no horizontal asymptote in the regime of 10^5 to 10^9 cycles. Ding et al. (Ref 20) investigated the effects of hydrogen on fatigue crack growth behavior of Ti-6Al-4V and reported that, at a higher stress ratio of 0.5; hydrogen embrittlement enhanced cracking and alleviated the effect of crack deflections in Ti-6Al-4V. Wang et al. (Ref 21) reported the influences of precrack orientations in welded joint of Ti-6Al-4V on fatigue crack growth. It was found that the specimen with a precrack along the weld center line exhibited lower fatigue crack propagation rate and significantly higher threshold stress intensity than the base metal specimen. No matter the precrack was initiated in the center of the weld, near the fusion-line or in HAZ, the fatigue crack propagation rates in the initial stage were slower than that of the base metal. Although crack path fluctuations and crack bifurcations also occurred frequently in martensite structures of FZ, in the initial propagation stage, the crack in the specimen with a precrack along the weld center line propagated by striation mechanism, not cleavage mechanism.

From the literature review, it is understood that extensive research work has been carried out on fatigue behavior of forgings and bars of Ti-6Al-4V alloy. Most of the published information focuses on the effect of stress ratio, surface, phase morphology residual stress, and crack growth behavior. However, there is no literature available comparing the fatigue, tensile properties and microstructural features of GTAW, LBW, and EBW joints of Ti-6Al-4V alloy. Hence, the present investigation was carried out to compare the fatigue behavior, tensile properties, and microstructural characteristics of GTAW, LBW, and EBW joints in the Ti-6Al-4V alloy.

2. Experimental Work

The rolled plates of 5.4 mm thick Ti-6Al-4V alloy were used as base metal (BM) to fabricate the joints. The chemical composition and mechanical properties of the BM are presented in Table 1 and 2, respectively. The optical micrograph of BM is shown in Fig. 1. It contains bimodal structure of elongated grains of "α" (light etched) and transformed "β" (dark etched) containing some amount of acicular "α." The "β" phase is distributed at the boundaries of the "α" phase (Ref 22). A Single "V" butt joint configuration was prepared as shown in Fig. 2(a) to fabricate the joints using the GTAW process. Square butt joint configuration was prepared as shown in Fig. 2(b) to fabricate the joints using LBW and EBW processes. The optimized welding conditions (presented in Table 3) were used to fabricate the joints. Welding trials were conducted and the joints were sectioned for micrographic examinations to find out the complete joint penetration (CJP) and defect-free joints. The trial which produced defect-free CJP was considered as the optimized welding condition, the corresponding parameters are used to weld the joints. Necessary clamping and welding fixtures were used to avoid joint distortion during welding. The welding was carried out normal to the rolling direction of the base metal.

The welded joints were sliced as shown in Fig. 3(a), using wire-cut Electric Discharge Machining (WEDM) to prepare fatigue and tensile test specimens. Two different fatigue

Table 1 Chemical composition of base metal (wt.%)

Al	V	Fe	O	N	C	Ti
6.38	4.07	0.19	0.17	0.008	0.012	Bal.

Table 2 Mechanical properties of base metal

Yield strength, MPa	Ultimate tensile strength, MPa	Elongation in 50 mm gauge length, %	Hardness in HV at 0.05 kg
969	1002	12.7	372

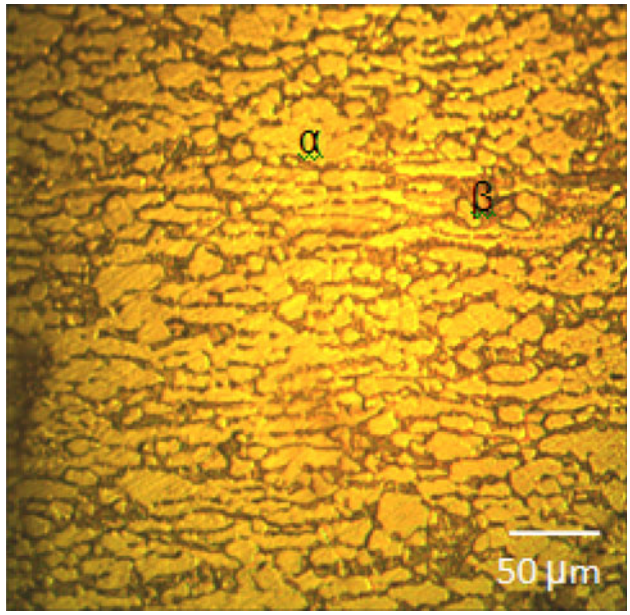

Fig. 1 Optical micrograph of base metal

specimens were prepared to evaluate the fatigue properties as per ASTM E467-08 specifications. Hourglass type (smooth) specimens were prepared as shown in Fig. 3(b) to evaluate fatigue limit and notched specimens were prepared as shown in Fig. 3(c) to evaluate the fatigue notch factor and notch sensitivity factor. The weld beads of the joints were machined and the effect of bead profile was eliminated in this study. The smooth tensile specimens were prepared (Fig. 3d) to evaluate yield strength, tensile strength, percentage elongation. The tensile specimens were prepared as per the ASTM E8M-04 standard guidelines. The photographs of fabricated joints and prepared fatigue testing specimens are presented in Fig. 4.

The fatigue testing experiments were conducted at five different stress levels and all the experiments were conducted under uniaxial tensile loading condition (tension-tension, stress ratio = 0.1, frequency = 10 Hz) using servo hydraulic fatigue testing machine (Make: INSTRON, UK; Model: 8801). The fractured surfaces of fatigue tested (both smooth and notched) specimens were analyzed through scanning electron microscope (HITACHI, S400N). Tensile testing was carried out using 100 kN, electro mechanical controlled universal testing machine (Make: FIE-Blue star, India; Model: UNITEK-94100). The 0.2% offset yield strength was derived from the load displacement diagram obtained using an extensometer. Hardness measurements were done across the weld center line by Vickers micro hardness tester (SHIMADZU, Japan Model: HMV-2T) with 0.05 kg load and 15 s dwell time. The specimens for metallographic examination were sectioned to the required sizes from the joint regions and polished using different grades of emery papers. Final polishing was done using the diamond compound (1 μm particle size) in the disk polishing machine. Specimens were etched with Kroll's reagent to reveal the micro- and macrostructure. The microstructural analysis was done by optical microscope (MEIJI, Japan; Model: ML7100).

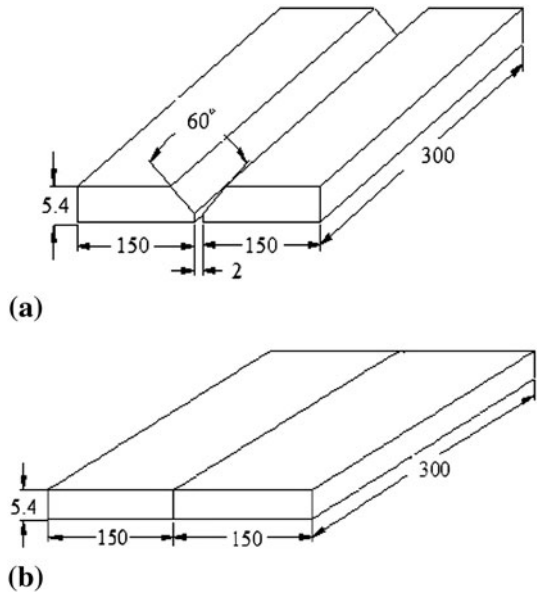

Fig. 2 Dimensions of Joint configuration. (a) Single 'V' butt joint (for GTAW) and (b) Square butt joint (for LBW and EBW) (all dimensions are in "mm")

3. Results

3.1 Fatigue Properties

Three specimens were tested at each stress level and the average result is used to plot *S-N* curves as shown in Fig. 5. The *S-N* curve in the high cycle fatigue region is generally described by the Basquin equation (Ref 23).

$$S^n N = A \qquad \text{(Eq 1)}$$

where S is the stress amplitude, N is the number of cycles to failure, and, n and A are empirical constants. Each *S-N* curve shown in Fig. 5 can be represented by the above equation. From those equations, the empirical constants n (slope of the curve) and A (intercept of the curve) were evaluated and they are presented in Table 4. When comparing the fatigue strengths of different welded joints subjected to similar loading, it is convenient to express fatigue strength in terms of the stresses corresponding to particular lives, for example 10^5, 10^6, and 10^7 cycles on the mean *S-N* curve. The choice of reference life is quite arbitrary. For these reasons, in this investigation, fatigue strength of welded joints at 1×10^6 cycles was taken as a basis for comparison. The stress corresponding to 1×10^6 cycles was taken as an indication of the endurance limit and it was evaluated for all the joints and is presented in Table 4. The effect of notches on fatigue strength was determined by comparing the *S-N* curves of notched and unnotched specimens. The data for notched specimens are usually plotted in terms of nominal stress based on the net section of the specimen. The effectiveness of the notch in decreasing the fatigue limit is expressed by the fatigue strength reduction factor or fatigue notch factor, K_f. The fatigue notch factor for all the joints was evaluated using the following expression (Ref 23).

Table 3 Welding parameters used to fabricate the joints

Parameters	GTAW	LBW	EBW
Machine	Lincoln, USA	DC035, Slab CO_2 laser from Rofin Sinar Laser, GmbH	Techmeta, France
Polarity	AC	…	DCEN
Filler metal	ERTi-5	…	…
Electrode	Tungsten	…	Tungsten
Shielding gas	100% Argon	100% Helium	100% Argon
Current	125 A	…	50 mA
Voltage	10 V	…	50 kV
Welding speed, mm/min	60	1500	650
Power	…	3500 W	…
Heat input, kJ/mm	1.25	0.14	0.231

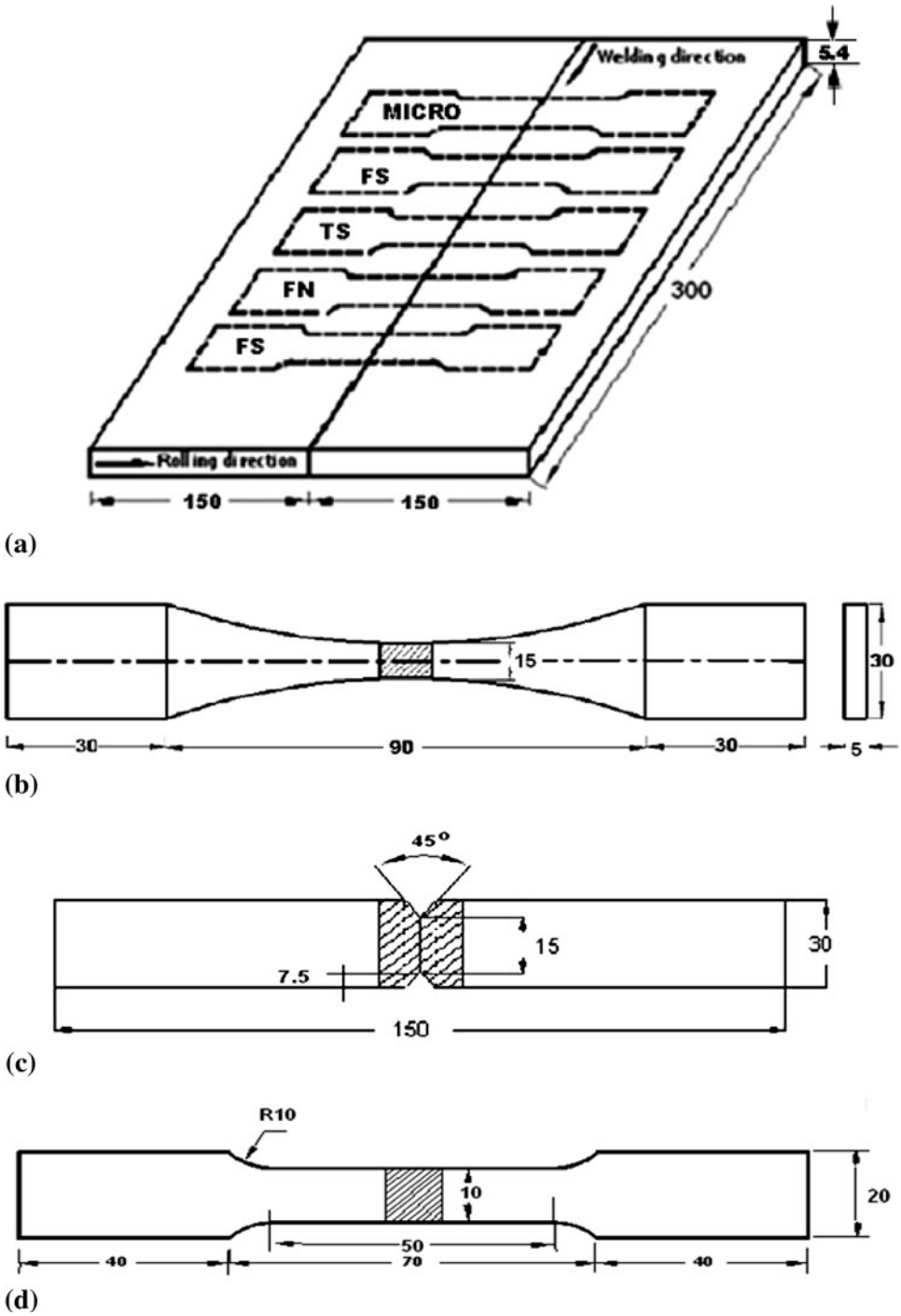

Fig. 3 Joint and specimen dimensions. (a) Scheme of welding with respect to rolling direction and extraction of specimens (FS, fatigue smooth; FN, fatigue notched; TS, tensile smooth; TN, tensile notched), (b) unnotched fatigue specimen, (c) notched fatigue specimen, and (d) unnotched tensile specimen (all dimensions are in "mm")

$$K_f = \text{Fatigue limit of unnotched specimen} / \text{Fatigue limit of notched specimen} \quad \text{(Eq 2)}$$

The notch sensitivity of a material in fatigue is expressed by q and it can be evaluated using the following expression (Ref 23).

$$q = K_f - 1/K_t - 1 \quad \text{(Eq 3)}$$

where K_t is the theoretical stress concentration factor and is the ratio of maximum stress to nominal stress. Using the above expression, fatigue notch sensitivity factor q was evaluated for all the joints and they are presented in Table 4.

From the results presented in Table 4, it is inferred that the BM endured more number of cycles than all the joints. Of the three welded joints, the LBW joints exhibited superior fatigue performance and it endured 63% more number of cycles than GTAW joints and 29% more number of cycles than EBW joints in the unnotched conditions. Similarly, LBW joint endured 77 and 33% more number of cycles than GTAW joints and EBW joints, respectively, in the notched conditions. The slope of the

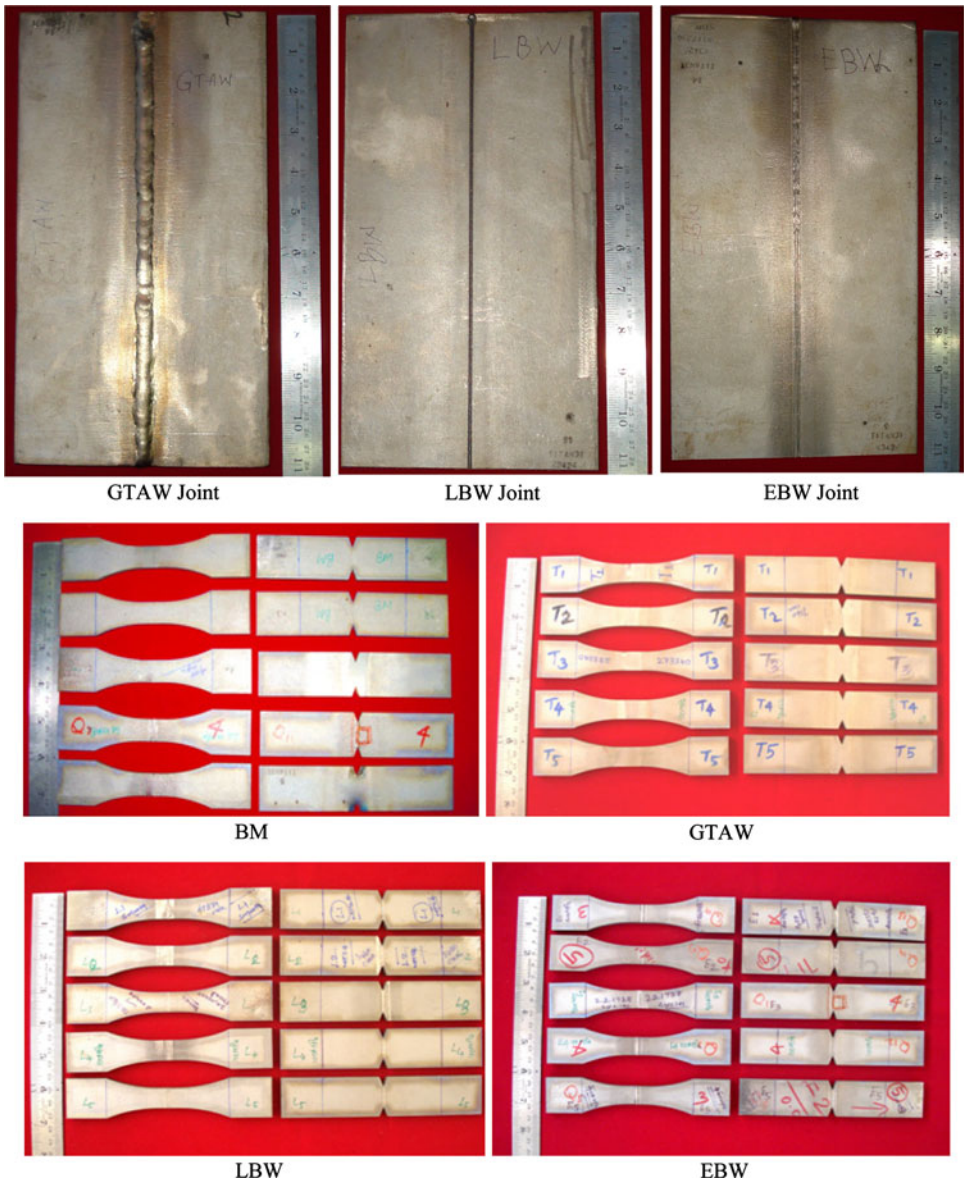

Fig. 4 Photographs of joints and fatigue tested specimen

S-N curve (Basquin Constant) is another measure to understand the fatigue performance of welded joints. If the slope of the *S-N* curve is smaller, then the fatigue life will be higher and vice versa. This could be the reason for LBW joint with a minimum slope (−0.530) exhibits maximum endurance stress of 180 MPa than GTAW and EBW joints. Thus, the joints fabricated using LBW process exhibited superior performance than the joints fabricated using GTAW and EBW processes in both notched and unnotched conditions. Reduction in fatigue strength due to the presence of square V-notch was evaluated by fatigue notch factor and the notch sensitivity factor. The notch sensitivity factor of the GTAW joints is found to be higher than the other joints. The notch sensitivity factor of LBW joint is found to be lower than the other joints.

3.2 Fracture Surface

The location of failure in all the fatigue tested specimens was at the weld metal. The fractured surface of the fatigue tested specimens of base metal and welded joints was analyzed using a scanning electron microscope and the fractographs are displayed in Fig. 6, 7. The mode of failure for the fatigue tested (smooth) BM and the welded joints are a combination of ductile with microvoid coalescence called ductile rupture (DR) and tearing topography surfaces (TTS) in BM, LBW, and GTAW joints. Tearing topography surfaces are generally characterized by relatively smooth, often flat, areas or facets that usually contain thin tear ridges (Fig. 6a, c, d). Figure 6(a) shows the finer equiaxed dimple structure. TTS fracture appears to be the result of a microplastic tearing process that operates on a very small (submicron) scale (Ref 24). The TTS fractures do not exhibit as much plastic deformation as dimple rupture, although they are often observed in combination with dimples. A typical State I fatigue fracture is observed in GTAW joint (Fig. 6b). State I fatigue fracture surfaces are faceted, often resemble cleavage, and do not exhibit fatigue striations. Stage I fatigue is normally observed on high-cycle low-stress fractures and is frequently absent in low cycle high-stress fatigue. TTS and DR

are evidenced in LBW joint (Fig. 6c). Many small voids, which bear little resemblance to conventional dimples, are visible among the small facets (Ref 25). TTS, DR, and cleavage mode of fracture were observed in EBW joint (Fig. 6d).

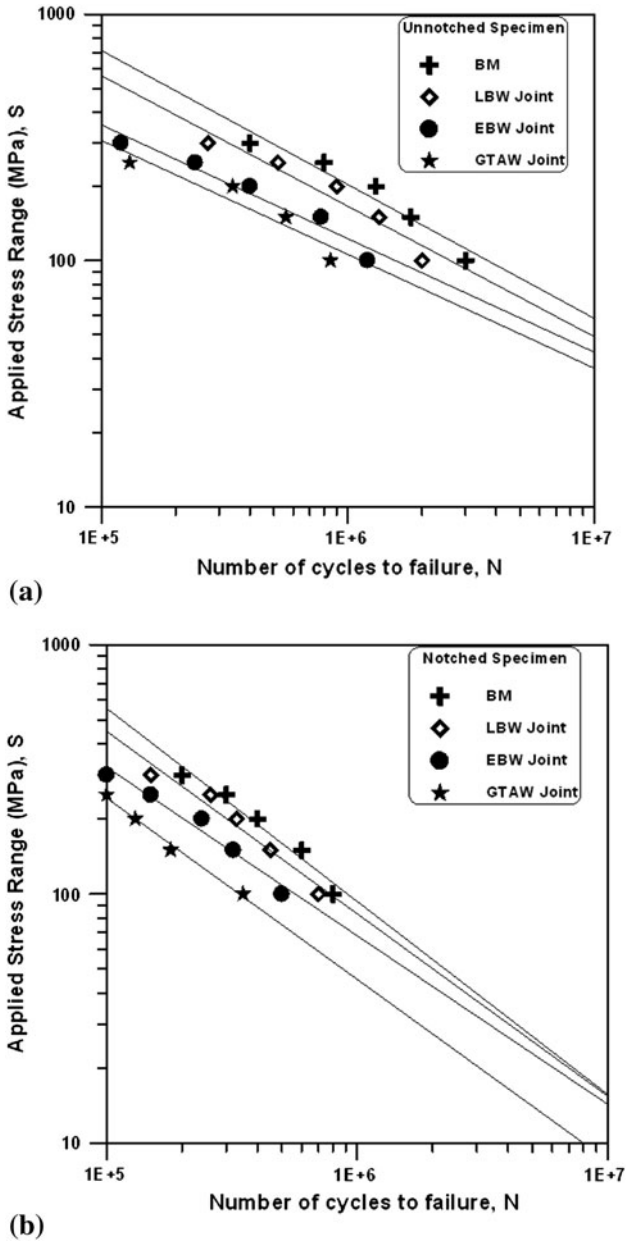

Fig. 5 *S-N* behavior of base metal and welded joints. (a) Unnotched fatigue test results and (b) notched fatigue test results

Complete TTS fracture mode was observed in notched fatigue BM (Fig. 7a). The presence of micro-cracks in addition with the TTS is observed in the notched GTAW fatigue specimen fracture surface (Fig. 7b). A combination of TTS and DR are observed in the notched LBW fatigue specimen. Fatigue striations and TTS are observed in the notched EBW (Fig. 7d) fatigue specimen. Fatigue fractures generated during Stage II fatigue usually exhibit crack-arrest marks known as fatigue striations which are a visual record of the position of the fatigue crack front during crack propagation through the material. In the entire notched fatigue tested specimen, the fracture is observed to be a mixture of shear rupture and transgranular cleavage.

3.3 Tensile Properties

The transverse tensile properties such as yield strength, tensile strength, and percentage of elongation of Ti-6Al-4V alloy joints were evaluated. In each condition, three specimens were tested, and the average of three results is presented in Table 5. The yield strength and tensile strength of unwelded parent metal are 969 and 1002 MPa, respectively. But the yield strength and tensile strength of GTAW joints are 890 and 940 MPa, respectively. This indicates that there is a 6% reduction in strength values due to GTAW process. Similarly, the yield strength and tensile strength of LBW joints are 960 and 985 MPa, respectively which is 2% lower when compared to parent metal. However, the yield strength and tensile strength of EBW joints are 950 and 1000 MPa, respectively. Of the three welded joints, the joints fabricated by the LBW process exhibited higher strength values, and the enhancement in strength value is approximately 6% when compared to GTAW joints and 2% when compared to LBW joints.

Elongation of unwelded parent metal is 12.7%. But the elongation of GTAW joints is 10.15%. This suggests that there is a 20 % reduction in ductility due to GTAW process. Similarly, the elongation of LBW joints is 15%, which is 18.1 % higher when compared to the parent metal. However, the elongation of EBW joints is 7.7 %. Of the three types of welded joints, the joints fabricated by LBW exhibited higher ductility values, and the improvement in ductility is approximately 48% compared to GTAW joints and 95% compared to EBW joints.

3.4 Hardness

The hardness across the weld cross section was measured using a Vickers Micro-hardness testing machine, and the values are presented in Table 5. The hardness of BM (unwelded parent metal) in its initial condition is 372 VHN (Table 2). But the hardness of the GTAW, LBW, and EBW joints in the weld metal region were 390, 463, and 488 VHN, respectively. This suggests that the hardness is increased by 18 VHN, 91 VHN, and 116 VHN in the weld metal region of GTAW, LBW, and

Table 4 Fatigue properties of the base metal and welded joints

Joint type	Slope of the *S-N* curve, n	Intercept of the *S-N* curve, A	Fatigue strength of the unnotched specimens at 1×10^6 cycles, MPa	Fatigue strength of the notched specimens at 1×10^6 cycles, MPa	Fatigue notch factor, K_f	Notch sensitivity factor, q
BM	−0.544	374641	210	100	2.10	0.20
GTAW	−0.460	63113	110	45	2.44	0.26
LBW	−0.530	252701	180	80	2.25	0.23
EBW	−0.462	72131	140	60	2.33	0.24

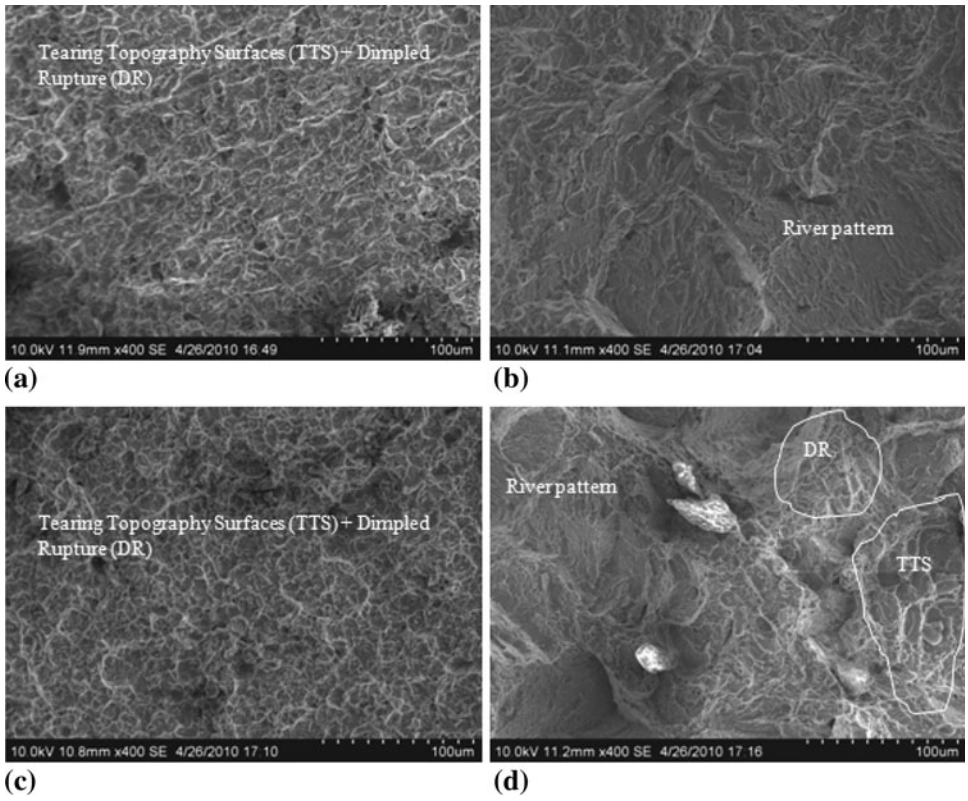

Fig. 6 Fractographs of fatigue (smooth) tested specimen. (a) BM, (b) GTAW joint, (c) LBW joint, and (d) EBW joint

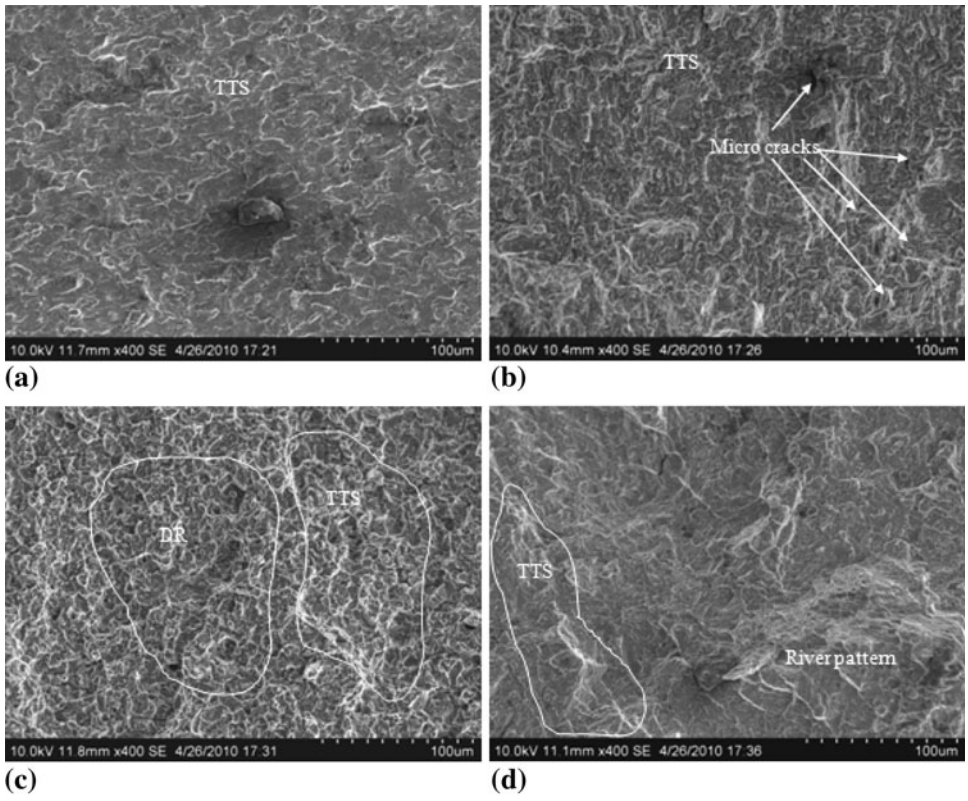

Fig. 7 Fractographs of fatigue (notched) tested specimen. (a) BM, (b) GTAW joint, (c) LBW joint, and (d) EBW joint

Table 5 Transverse tensile properties and hardness of welded joints

	0.2% offset Yield strength, MPa	Ultimate tensile strength, MPa	Elongation in 50 mm gauge length, %	Weld metal Hardness in HV at 0.05 kg
GTAW	890	940	10.15	390
EBW	950	1000	7.70	488
LBW	960	985	15.00	463

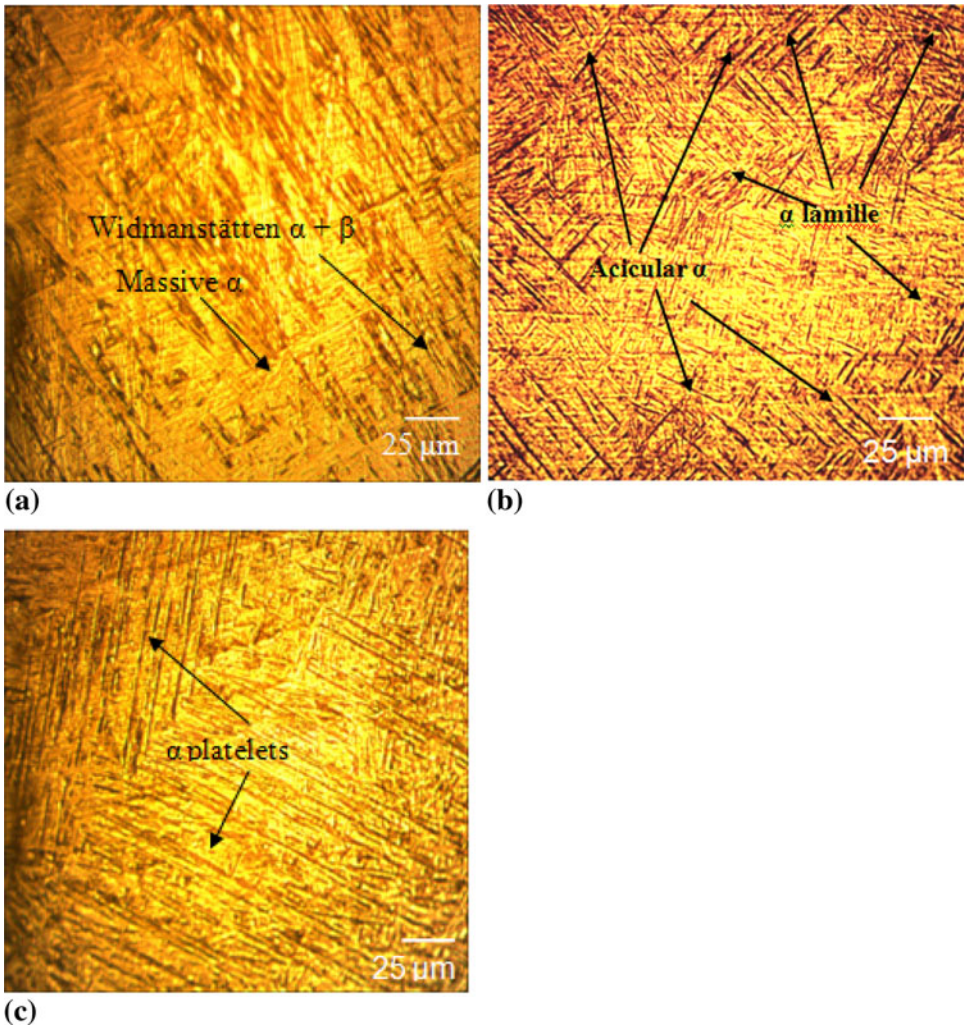

Fig. 8 Optical micrograph of weld metals. (a) GTAW, (b) LBW, and (c) EBW

EBW joints, respectively, due to welding thermal cycle and the resultant microstructure. This is 1.04, 1.24, and 1.32 times greater than that of the BM for GTAW, LBW, and EBW joints, respectively. Hardness has a direct influence over the yield strength, tensile strength, and ductility of the joints and hence, the resultant fatigue behavior of the joints is also affected.

3.5 Microstructure

Optical micrographs of weld metal region of the joints are presented in Fig. 8. Fusion zone microstructure of GTAW joint (Fig. 8a) containing the coarse serrate and acicular α structures of grain boundary α, massive α, and Widmanstätten α + β (Ref 26). The weld fusion zone in titanium alloys is characterized by coarse, columnar prior-beta grains that originate during weld solidification. The size and morphology of these grains depend on the nature of the heat flow that occurs during weld solidification. The fusion-zone beta grain size depends primarily on the weld energy input, with a higher energy input promoting a larger grain size. The reason for the grain coarsening of the GTAW joint can be justified to the heat input involved in this process. The heat input supplied here is 1.25 kJ/mm (Table 3) which is higher when compared with the LBW and EBW processes. The higher heat input leads to longer cooling time resulting in coarse grained structure of massive α, and Widmanstätten α + β. Three-dimensional or mixed two-dimensional/three dimensional heat-flow conditions, such as those present in single-pass and multi pass GTAW weldments, promote this formation of more complex, multidirectional beta grain morphologies. At the lower cooling rates associated with

GTAW (10 to 100 °C/s, or 18 to 180°F/s), a coarser structure of Widmanstätten alpha plus retained beta, or a mixture of this structure and alpha-prime (Ref 12) The microstructure of LBW joint shows that fine lamellar and acicular "α" structure (Fig. 8b). The heat input associated with LBW process is 0.14 kJ/mm which is the lowest of the three processes considered. Lowest heat input leads to faster cooling rate (100-10,000 °C/s or 180 to 18,000°F/s) and finer microstructure of α lamellae. Figure 8(c) reveals the EBW joint microstructure and it shows the serrate and regular plate-shaped α structures. The formation of the acicular grains is due to the fast cooling rate by LBW process and the plate-like α is due to the slow cooling rate in EBW process (Ref 27). The heat input of the EBW process is (0.231 kJ/mm) intermediate between GTAW and LBW processes. Heat input of EBW process is relatively higher than LBW process. This leads to slower cooling in Electron Beam (EB) welds than Laser Beam (LB) welds and resulted "α" platelets in EB welds instead of lamellae resulted in LB welds, because the lamellae are allowed to grow further.

4. Discussion

Transverse tensile properties of the welded joints presented in Table 5 indicates that the LBW joints are exhibiting higher yield strength properties compared to GTAW and EBW joints. During tensile test, all the specimens invariably failed in the weld metal. This indicates that the weld metal is comparatively weaker than other regions and hence the joint properties are controlled by weld metal chemical composition and microstructure. The higher strength of the BM is mainly attributed to the presence of elongated grains of "α" and transformed "β" containing some amount of acicular "α." The microstructure of the weld metal also plays a major role in deciding the joint properties of titanium alloys and it is dictated by the amount, size, shape, and morphology of "α" phase and density of α-β interfaces. Mechanical properties of composite weld structures in titanium alloys depend on structural characteristics of each weld region, which in turn depend on the specific thermal cycle(s) imposed during welding. In addition to prior-"β" grain size, weld zone mechanical properties in Ti-6Al-4V are significantly influenced by the manner in which the high-temperature, body-centered-cubic "β" phase transforms on cooling to the low-temperature, hexagonal-close-packed phase. Characteristics of this "transformed-β" microstructure depend principally on the cooling rate from above the beta transus temperature, which is correspondingly influenced by the welding process, process parameters, and other welding conditions (such as workpiece geometry and fixturing). The high cooling rates associated with low-energy-input welding processes such as LBW and EBW promotes transformation of beta to alpha-prime martensite. This extremely fine, acicular transformation product exhibits high strength and hardness. At the lower cooling rates associated with GTAW a coarser structure of Widmanstätten "α" plus retained "β," or a mixture of this structure and alpha-prime, is produced, which exhibits yield and tensile strengths inferior to those base metal and a ductility and toughness greater than those of an entirely martensitic microstructure (LBW and EBW joints) (Ref 12).

The microstructure of the weld metal is influenced by the heat input of the welding processes. Of the three welding processes used in this investigation to fabricate the joints, the GTAW process recorded higher heat input compared to the LBW and EBW processes (Table 3). Generally, higher heat input will lead to slower cooling rate and slow cooling rate will result in coarse microstructure. The lower strength of GTAW joint may be attributed to the presence of coarse serrate structures of grain boundary α, massive α, and Widmanstätten α + β. The moderate yield strength of EBW joint could be attributed to the weld metal microstructure containing fine serrate and regular plate-shaped "α" microstructures. Higher yield strength is achieved by the LBW joint due to the fine lamellar and acicular morphology of the joint. In this joint, the presence of martensitic structure is also observed. It was reported that cooling rates higher than 410 °C/s are usually required for Ti-6Al-4V alloy to attain a completely martensitic structure (Ref 28). The high self-quenched rate associated with the laser beam welding process certainly promotes the diffusion less transformation of the "β" phase in to martensitic microstructure.

The microstructures of the weld metal region will have greater influence on the fatigue performance of the joint than weld bead geometry, joint design, etc. Microstructure invariably affects the fatigue strength by increasing the propensity for crack nucleation and its early growth, causing the ultimate failure of the joint. In addition to α grain size, degree of age hardening, and oxygen content, the fatigue properties of two-phase α + β alloys are strongly influenced by the morphology and arrangements of the two phases "α" and "β." Equiaxed microstructure is present in BM whereas lamellar, acicular, and bimodal microstructures (primary α in a lamellar matrix) were yielded in LBW, EBW, and GTAW joints (Ref 12). In lamellar microstructures (Fig. 8b and c), fatigue cracks initiate at slip bands within "α" lamellae or at "α" along prior "β" grain boundaries (Ref 29). Since the resistance to dislocation motion as well as fatigue crack initiation depends on the "α" lamellae width, there is a direct correlation between fatigue strength and yield stress. For equiaxed structures, fatigue cracks nucleate along slip bands within "α" grain (Fig. 1). Thus, fatigue strength correlates directly with the grain size-dependent yield stress. In duplex structures, fatigue cracks can either initiate in the lamellar matrix, at the interface between the lamellar matrix and the primary 'α' phase, or within the primary α phase (Fig. 8a). The precise crack initiation site depends on the cooling rate (Ref 24), and the volume fraction and size of the primary "α" phase (Ref 28, 30). For a lamellar microstructure, lamellar width should be considered instead of grain size.

A reduction of prior β grain size in lamellar microstructures and a reduction of the primary "α" volume fraction in duplex structures increase both LCF life as well as fatigue strength (Ref 31, 32). Simultaneously, this structural modification increases the resistance to crack growth. Therefore, the fine-grained lamellar microstructure shows superior resistance to crack growth behavior over the coarse grained lamellar structure, while for duplex structures the lower primary α volume fraction is superior to the higher one. The latter can probably be explained by the (near) absence or lower presence of agglomerates of primary α grains and simultaneously reduced primary α volume fraction. This primary α cluster can act as large single grains, which are easy for micro-cracks to propagate through (Ref 31-33). Thus the joints consisting of coarse lamellar (EBW) and bimodal (GTAW) yields lower fatigue strength than the joint having fine lamellar microstructure (LBW). The presence of fine lamellar microstructure in the

weld metal enhanced the yield strength and ductility of the LBW joint. Fine lamellar in addition with acicular morphology (inter locking nature of multi directionally oriented grains) play an important role for the resultant tensile and ductility of the LBW joint. It is well known that a structure containing a large percentage of lamellar "α" offers greater resistance to crack growth than equiaxed structures. This can be usually ascribed to the fact that crack path deviations and bifurcations can occur more easily in plate-like structures (Ref 34). The improvement in the yield strength may be one of the reasons for higher fatigue strength of LBW joint. Similarly, the higher ductility (higher elongation) may be one of the reasons for lower fatigue notch sensitivity of the LBW joint.

5. Conclusions

In this article, the fatigue properties of GTAW, LBW, and EBW joints of Ti-6Al-4V titanium alloy were evaluated. From this investigation, the following important conclusions are derived:

(i) Of the three joints, the joints fabricated by LBW process exhibited higher fatigue strength (180 MPa) than EBW (140 MPa), and GTAW (110 MPa) joints.
(ii) Of the three joints, the LBW joint is less sensitive (0.23) to notches under fatigue loading than EBW (0.24) and GTAW (0.26) joints.
(iii) Higher yield strength and higher ductility due to the presence of very fine lamellar-shaped "α" microstructure in the weld metal are the main reasons for the superior fatigue performance of the LBW joints when compared to GTAW and EBW joints.

Acknowledgments

The authors wish to record their sincere thanks to the Combat Vehicle Research and Development Establishment (CVRDE), Avadi, Chennai, for providing financial support to carry out this investigation through a Contract Acquisition for Research Services project, No. CVRDE/MMG/09-10/0043/CARS. The authors register their sincere thanks to Defense Research & Development Laboratory (DRDL), Hyderabad and Centre for Laser Processing of Materials (CLPM), ARCI, Hyderabad for effective fabrication of the joints. The authors wish to place their sincere thanks to Mr. M. Balakrishanan, Project Associate, CEMAJOR, Annamalai University for his help in carrying out this investigation.

References

1. T. Nykanen, X. Li, T. Bjork, and G. Marquis, A Parametric Fracture Mechanics Study of Welded Joints with Toe Cracks and Lack of Penetration, *Eng. Fract. Mech.*, 2005, **72**, p 1580
2. D. Ju, Potential Applications of Titanium and its Alloys, *Rare Metal Mater. Eng.*, 1997, **1**, p 7
3. L. Guozhen, Z. Lian, and D. Ju, Newer Materials for High Temperature and Corrosion Resistance Applications, *Rare Metal Mater. Eng.*, 1997, **5**, p 1
4. G. Disheng, *Nonferrous Metal Welding*, Mechanical Industry Press, Beijing, 1987, p 206
5. F. Caiazzo, F. Curcio, G. Daurelio, and F.M.C. Minutolo, Ti–6Al–4V Sheets Lap and Butt Joints Carried Out by CO2 Laser: Mechanical and Morphological Characterization, *J. Mater. Process. Technol.*, 2004, **149**(1–3), p 546–552
6. G. Casalino, F. Curcio, and F.M.C. Minutolo, Investigation on Ti–6Al–4V Laser Welding Using Statistical and Taguchi Approaches, *J. Mater. Process. Technol.*, 2005, **167**(2–3), p 422–428
7. M. Balasubramanian, V. Jayabalan, and V. Balasubramanian, A Mathematical Model to Predict Impact Toughness of Pulsed-Current Gas Tungsten Arc-Welded Titanium Alloy, *Int. J. Adv Manuf Technol*, 2008, **35**, p 852–858
8. S. Zhang, X. Lin, J. Chen, and W. Huang, Heat Treated Microstructure and Mechanical Properties of Laser Solid Forming of Ti-6Al-4V alloy, *Rare metals*, 2009, **28**(6), p 537
9. N. Saresh, M. Gopalakrishna Pillai, and Jose. Mathew, Investigations into the Effects of Electron Beam Welding on Thick Ti–6Al–4V Titanium Alloy, *J. Mater. Process. Technol.*, 2007, **192–193**, p 83–88
10. N.J. Noolua, H.W. Kerra, Y. Zhoua, and J. Xieb, Laser Weldability of Pt and Ti Alloys, *Mater. Sci. Eng. A*, 2005, **397**, p 8–15
11. M. Balasubramanian, V. Jayabalan, and V. Balasubramanian, Prediction and Optimization of Pulsed Current Gas Tungsten Arc Welding Process Parameters to Obtain Sound Weld Pool Geometry in Titanium Alloy Using Lexicographic Method, *ASM International, JMEPEG*, 2009, **18**, p 871–877
12. "ASM Hand Book Volume 6—Welding, Brazing and Soldering," p740-754, 1289-1230
13. K. Keshava Murthy and S. Sundaresan, Fatigue Crack Growth Behavior in a Welded α–β Ti-Al-Mn Alloy in Relation to the Microstructural Features, *Mater. Sci. Eng. A*, 1997, **222**, p 201–211
14. V.K. Saxena and V.M. Radhakrishnan, Effect of Phase Morphology on Fatigue Crack Growth Behavior of a-b Titanium Alloy—A Crack Closure Rationale, *Metall. Mater. Trans. A*, 1998, **29A**, p 245–261
15. K.H. George, T. Nicholas, and D.B. Lanning, Notch Size Effects in HCF behavior of Ti-6Al-4V, *Int. J. Fatigue*, 1999, **21**, p 643–652
16. S.R. Thompson, J.J. Ruschau, and T. Nicholas, Influence of Residual Stresses on High Cycle Fatigue Strength of Ti–6Al–4V Subjected to Foreign Object Damage, *Int. J. Fatigue*, 2001, **23**, p S405–S412
17. B.L. Boyce and R.O. Ritchie, Effect of Load Ratio and Maximum Stress Intensity on the Fatigue Threshold in Ti-6Al-4V, *Eng. Fract. Mech.*, 2001, **68**, p 129–147
18. L.W. Tsay, Y.P. Shan, Y.-H. Chao, and W.Y. Shu, The Influence of Porosity on the Fatigue Crack Growth Behavior of Ti–6Al–4V Laser Welds, *J. Mater. Sci.*, 2006, **41**, p 7498–7505
19. J.H. Zuo, Z.G. Wang, and E.H. Han, Effect of Microstructure on Ultra-High Cycle Fatigue Behavior of Ti–6Al–4V, *Mater. Sci. Eng. A*, 2008, **473**(1–2), p 147–152
20. Y.S. Ding, L.W. Tsay, and C. Chen, The Effects of Hydrogen on Fatigue Crack Growth Behaviour of Ti–6Al–4V and Ti–4.5Al–3V–2Mo–2Fe alloys, *Corrosion Science*, 2009, **51**(6), p 1413–1419
21. X. Wang, Q. Shi, X. Wang, and Z. Zhang, The Influences of Precrack Orientations in Welded Joint of Ti–6Al–4V on Fatigue Crack Growth, *Mater. Sci. Eng. A*, 2010, **527**(4–5), p 1008–1015
22. X. Cao and M. Jahazi, Effect of Welding Speed on Butt Joint Quality of Ti–6Al–4V Alloy Welded Using a High-Power Nd:YAG Laser, *Opt. Lasers Eng.*, 2009, **47**, p 1231–1241
23. E. George, *Dieter, Mechanical Metallurgy*, 3rd ed., McGraw-Hill Publishing, New York, 1988, p 376–431
24. A.W. Thompson and J.C. Chesnutt, Identification of a Fracture Mode: The Tearing Topography Surface, *Metall. Trans. A.*, 1979, **10A**, p 1193
25. "ASM Hand Book Volume 12—Fractography," p 768-793
26. "ASM Hand Book Volume 9—Metallography & Microstructures, p 968-1015
27. Q. Yunlian, D. Ju, H. Quan, and Z. Liying, Electron Beam Welding, Laser Beam Welding and Gas Tungsten Arc Welding of Titanium Sheet, *Mater. Sci. Eng.*, 2000, **A280**, p 177–181
28. T. Ahmed and H.J. Rack, Phase Transformation During Cooling in α + β Titanium Alloys, *Mater. Sci. Eng.*, 1998, **A243**, p 206–211
29. T. Mohandas, D. Banerjee, and V.V. Kutumba Rao, Fusion Zone Microstructure and Porosity in Electron Beam Welds of an a + b Titanium Alloy, *Metal. Trans.*, 1998, **30A**, p 789–798
30. G. Magudeeswaran, V. Balasubramanian, T.S. Balasubramanian, and G. Madhusudhan Reddy, Effect of Welding Consumables on Tensile Impact Properties of Shielded Metal Arc Welded High Strength, Quenched and Tempered Steel Joints, *Sci. Technol. Weld. Join.*, 2008, **13**, p 97–105
31. A. Berg, J. Kiese, and L. Wagner, Effect of Beta Grain Size on Mechanical Properties of Lamellar Microstructures in Timetal-1100,

Light-Weight Alloys for Aerospace Applications III, E.W. Lee, K.V. Jata, N.J. Kim, and W.E. Frazier, Ed., TMS, Warrendale, 1995, p 407

32. J. Lindemann, A. Styczynski, and L. Wagner, Fatigue Properties, *Light-Weight Alloys for Aerospace Applications III*, E.W. Lee, K.V. Jata, N.J. Kim, and W.E. Frazier, Eds., TMS, Warrendale, 1995, p 391
33. C. Leyens and M. Peters, Eds., Titanium and Titanium Alloys (Fundamentals and Applications), Wiley-VCH Verlag GmbH & Co. KGaA, Weinheim, 2003, ISBN: 3-527-30534-3, p 153–186
34. G.R. Yoder, L.A. Cooley, and T.W. Crooker, Quantitative Analysis of Microstructural Effects on Fatigue Crack Growth in Widmanstätten Ti-6A1-4V and Ti-8Al-1Mo-1V, *Eng. Fract. Mech.*, 1979, **11**, p 805